

Influence of soil-structure interaction on seismic responses of offshore wind turbine considering earthquake incident angle

Faria Sharmin^{1a}, Mosaruf Hussan^{1b}, Dookie Kim^{*1} and Sung Gook Cho^{2c}

¹Department of Civil Engineering, Kunsan National University, 558 Daehak-ro, Kunsan, Jeonbuk 54150, Republic of Korea

²Innose Tech Company Limited, Republic of Korea

(Received October 10, 2016, Revised May 31, 2017, Accepted July 20, 2017)

Abstract. Displacement response and corresponding maximum response energy of structures are key parameters to assess the dynamic effect or even more destructive structural damage of the structures. By employing them, this research has compared the structural responses of jacket supported offshore wind turbine (OWT) subjected to seismic excitations apprehending earthquake incidence, when (a) soil-structure interaction (SSI) has been ignored and (b) SSI has been considered. The effect of earthquakes under arbitrary angle of excitation on the OWT has been investigated by means of the energy based wavelet transformation method. Displacement based fragility analysis is then utilized to convey the probability of exceedance of the OWT at different soil site conditions. The results show that the uncertainty arises due to multi-component seismic excitations along with the diminution trend of shear wave velocity of soil and it tends to reduce the efficiency of the OWT to stand against the ground motions.

Keywords: offshore wind turbine; soil-structure interaction; incident angle; wavelet transformation; fragility curve

1. Introduction

Over the last decades, offshore wind turbines (OWTs) associated with jacket foundation, subjected to perplexed environmental circumstance, have been installed at increasing water depths. As a consequence, the design and construction of foundations of the OWT are raising anomalous challenges for the complicated environmental conditions (Kuo *et al.* 2012). The turbine with the jacket support structure (5MW-OC4 Jacket) (Jonkman *et al.* 2009) has been used in this study. A comparison of the response of a jacket supported OWT has been evaluated under wave loadings when (a) the soil-structure interaction (SSI) has been ignored, and (b) the SSI has been considered (Abhinav and Shaha 2015) without taking into account the seismic loads. Besides, a reliability analysis of the OWT support structure with the simulation of the SSI has been accomplished under earthquake by Kim *et al.* (2015). Dynamic SSI is the key factor to ascertain the dynamic behavior of a structure (Jayalekshmi *et al.* 2014, Hussan *et al.* 2017). Although many efficient investigations have been practiced in order to analyze the dynamic response of the OWT to the strong interaction of aerodynamic and

hydrodynamic loadings, still it requires more inspections of the seismic analysis owing to limited research with the SSI. SSI has an obvious impact on any gigantic structure installed in the seismic prone zone (Adhikari and Bhattacharya 2011). A pioneer work has been accomplished by executing the non-linear analysis of soil-pile-structure under seismic interaction (Cai *et al.* 2000). As well as, FAST simulation (Prowell *et al.* 2009) and HAWT, developed by the National Renewable Energy Laboratory (NREL) (Valamanesh and Mayers 2014), have been conducted to ascertain the seismic impact on the wind turbines. In many situations SSI has been modeled using lateral, rotational and cross coupling springs, which has been contrasted to uncoupled springs (Bhattacharya *et al.* 2013). In the present inquisition, the inertial interaction between soil and the turbine has been modeled by constituting a set of frequency-independent springs and dashpots based on the credible concept of Voigt viscoelastic cone model. (Ghaffar-Zade and Cahpel 1983).

Accomplishing a proper model of a structure and adopting a high precision method in the analysis are not only the key factors to validate the seismic analysis results but also the selection of seismic waves and evaluation of the seismic incidence. Even though, it is assumed that the direction of ground motions are symmetrical with the fixed structural reference axes in the seismic design. But the horizontal components of ground motion follow the different axes due to the angle of incidence, which may lead to different structural responses (Kojima and Takewaki 2015, 2016). A method has been introduced by Wilson and Button (1982) for the purpose of estimating the angle of incidence of earthquakes. Besides, Smeby and Kiureghian (1985) have presented a circumstantial numerical model to calculate the critical angle of incidence apprehending

*Corresponding author, Professor

E-mail: kim2kie@kunsan.ac.kr

^aMaster Student

E-mail: fariasharmin07@gmail.com

^bMaster Student

E-mail: razib.mosaruf@gmail.com

^cDirector

E-mail: sgcho@innostech.com

horizontal components of ground motion. The CQC3 rule for the assessment of the incident angle and the corresponding maximum response has been introduced by Menun and Der Kiureghian (1998). Thereafter, Zhu *et al.* (2000) have proposed a method to obtain the incidence angle by the spectrum analysis twice. Nguyen and Kim (2013) have determined the incident angle for the asymmetric-plan structures subjected to combinations of two or more earthquake response quantities. The present approach has considered the most favorable combination of the two horizontal recorded components for determining the incident angle in time domain.

The energy of the earthquakes acceleration, measured from the beginning to the end, is called the total input energy of this motion. As same as, the energy of structural response in time domain, obtained after persuading the earthquake analysis, is the total output energy of the structure. The input earthquake energy to a structure has a great consequence causing structural damage (Uang and Bertero 1990, Fukumoto and Tatewaki 2015). In many circumstances, the smoothed Fourier amplitude spectrum has been used to obtain the input energy of earthquake response (Kuwamura *et al.* 1994). However, structural safety under earthquakes cannot be estimated by the previously mentioned energy spectra defined only in the frequency domain (Li *et al.* 2009). Relatively this study has used the wavelet transform for time phenomenon in the transient process (Li and Sun 2003). In 1984 the wavelet analysis was first applied in the development of oil and gas industry. Consequently, a huge amount of investigation has been accomplished to develop the methodology of wavelet analysis. Furthermore, the wavelet tool is gaining more attention in the field of geotechnical earthquake engineering to analyze the non-stationary seismic response of dynamic analysis (Iyama and Kuwamura 1999, Chatterjee and Basu 2004). Besides for the few decades, the wavelet analysis has been used to detect the damage in concrete structure, bridge and plate structures for the purpose of health monitoring (Melhem and Kim 2003, He and Zhu 2015, Hajizadeh *et al.* 2016).

In recent years the displacement based fragility analysis is an effective conventional method, which is earning attention and applicability for the seismic risk assessment of the complicated structural system. More recently, Karantoni *et al.* (2014) have used Fragility analysis to observe the damage of masonry buildings induced by the strong earthquake. As well as, Nuta (2010) has investigated the seismic response analysis of the 1.65-MW Vestas turbines extensively, where the study has established the fragility curves by the incremental dynamic analysis. Therefore, in the case of the OWT Kim *et al.* (2014) has carried out an observation of the seismic fragility analysis of the 5MW offshore wind turbine. Thereafter, Mohammad *et al.* (2016) have done the fragility analysis of the 5MW OWT considering the coupling of aero-elastic and seismic interaction. Nevertheless, in these above studies the orientation of incident angle has not been considered with the SSI effects and the fragility analysis has been done with respect to the target displacement.

This work has enlightened the influence of the SSI on

the OWT considering (a) no SSI (b) hard clay (c) stiff clay and (d) soft clay subjected to multi-component seismic excitations oriented by the incident angle. Two cases have been evaluated: (1) total structural energy, calculated by the wavelet transformation method and (2) the failure probability of the OWT, established by the fragility analysis. In the first part, the numerical calculation has been performed to determine the incident angle of the input seismic actions. The wavelet transform based on the basic energy principle is then executed to estimate the total energy of the structure. The total energy of four different structural models varies for each selected angle of incidence of the input seismic actions. In order to accomplish the second aim, the multi-strip analysis (Bradley 2010, Iervolino *et al.* 2010) has been adopted to assess the seismic capacity of the OWT with the SSI and without the SSI for uni-directional excitations as well as for bi-directional excitations.

2. Simulation process

2.1 Numerical model

The recent investigation has been carried out adopting the standard jacket foundation supported NREL 5 MW reference OWT designed by NREL, numerically modeled in the OpenSees. Originally Vemula *et al.* (2010) have designed this support structure and Song *et al.* (2013) has used this design for the offshore code collaboration continuation (OC4) project at a water depth of 50 m and water density 1025 kg/m^3 . Based on the environmental condition, the wind and wave loads calculated by the FAST have been applied to the tower and the jacket nodes as external nodal forces and moments. In the case of tower modeling, the tower has been discretized into different 9 force beam-column elements and carrying the rotor nacelle assembly (RNA) lumped mass at the top of it. Besides, the jacket support structure subjected to the wave nodal loads has consisted of 64 nodes and 112 force beam-column elements. The interface nodes of the jacket rigidly connected to the transition piece (TP). The mass density, Young's and shear modulus and Poisson's ratio of TP considered as a density filling rectangular body are 1807 kg/m^3 , $2.1 \times 10^{11} \text{ kg/m}^2$, $8.08 \times 10^{10} \text{ kg/m}^2$ and 0.18 respectively. Young's ($2.1 \times 10^{11} \text{ N/m}^2$) and shear ($8.08 \times 10^{10} \text{ N/m}^2$) modulus, mass density (7850 kg/m^3) and Poisson's ratio (0.3) are even for all the types of jacket support structure and tower elements as well as. The geometric and the inertia parameters of the structure are listed in Tables 1-2. Fig. 1 shows the typical model and OpenSees model of the OWT.

Table 3 lists the natural frequencies of the finite element model (FEM) identified by OpenSees and corresponding mode shapes of the FEM are shown in Fig. 2. The exploration delineates good agreement with the natural frequencies of the FAST and echoes these findings leading to clear verification of the OpenSees model. In addition, the summation of reaction force at fixed supports has been found to be equivalent to the self-weight of the whole

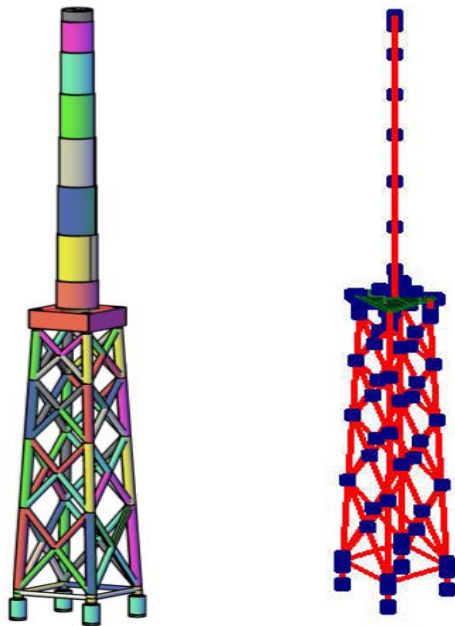
Table 1 Overview of the OWT

Parameter	Value
Tower base OD [m]	5.6
Tower base thickness [m]	0.032
Tower top OD [m]	4
Tower top thickness [m]	0.03
Tower Length [m]	68
TP dimension, [m ³]	9.6×9.6×4
RNA mass [kg]	350×10 ³
Tower mass [kg]	230×10 ³
TP mass [kg]	666×10 ³
Jacket mass [kg]	655.83×10 ³
Total OWT mass [kg]	1.9018×10 ⁶

Note: OD = Outer diameter, TP = Transition piece, RNA= Rotor nacelle assembly

Table 2 OWT jacket parameters

Parameter	Diameter (m)	Thickness (m)
X braces and Mud braces	0.8	0.02
Leg	1.20	0.05 (up to the 1st bay), 0.035-0.04 (TP)
Pile	2.08	0.491 (upper level), 0.069 (lower level)

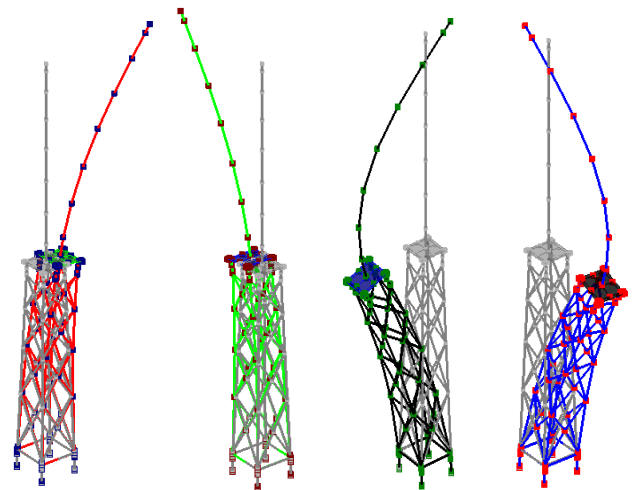


(a) Typical 3D model (b) OpenSees model

Fig. 1 Model of the OWT

Table 3 The natural frequency of FEM of the structures

Mode	Mode Shape	FAST (Hz)	OpenSees (Hz)
1	Fore-Aft mode	0.32	0.33
2	Side-Side mode	0.32	0.33
3	Fore-Aft mode	1.19	1.17
4	Side-Side mode	1.19	1.17



(a) First Side-Side (b) First Fore-Aft (c) Second Side-Side (d) Second Fore-Aft

Fig. 2 Mode shapes of the OWT

structure after executing the static analysis for the FEM only considering gravity loads.

2.2 Wind and wave loads

The structure has been subjected to the static wind and wave loads aligned with the dynamic earthquake loads. The wind and wave loads (IEC 61400-1 2010, IEC 61400-3 2009) calculated through the solver named FAST have been transferred to the OpenSees model. The FAST developed by the NREL is an aero-hydro-servo-elastic wind turbine dynamic analysis program. This solver is capable of performing a fully coupled analysis on floating OWTs. Maximum wind and wave loads obtained from the FAST have been applied as static forces on the tower nodes and the jacket nodes respectively. The loads consist of total six components of forces and moments in x , y and z -direction. The gravity of the structure has been accounted in the analysis.

2.3 Soil-structure interaction (SSI)

The structure and underlying the homogenous half-space soil stratum (Meek and Wolf 1993a, b) have been modeled separately and then combined together to comprise a physical model of the SSI beneath the jacket substructure. The process is widely recognized as a sub-structure methodology. Voigt viscoelastic cone model based on one-dimensional wave propagation has been used for the mathematical modeling of infinite soil medium (Wolf 1994). The model can describe the viscoelastic deformation of the soil medium by accounting total five degrees of freedoms, which have been considered in the cone model by permitting the sway and rocking motions about x and y directions and torsion about z direction. The inertial interaction between soil and the turbine has been modeled by constituting a set of frequency-independent springs and dashpots which are shown in Fig. 3.

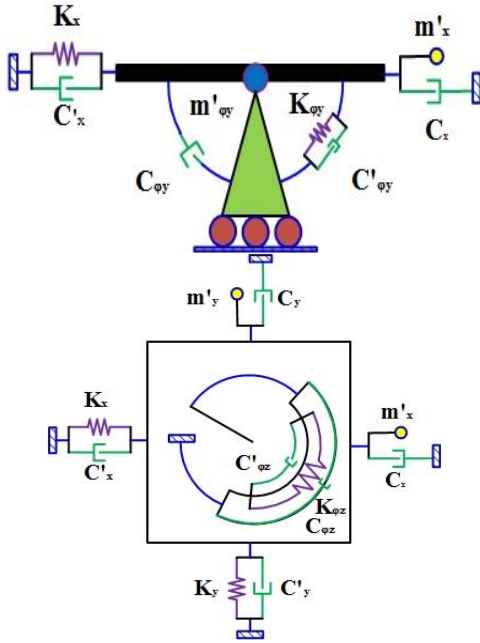


Fig. 3 Viscoelastic cone model

Expressions for the soil foundation model properties such as spring stiffness, viscous damping coefficient, and added masses are presented by using Eqs. (1)-(2)

$$K = \frac{\rho V^2 A_0}{z_0}, \quad C = \rho V A_0, \quad C' = 2 \frac{\zeta_0}{\omega_0} K, \quad (1)$$

$$m' = \frac{\zeta_0}{\omega_0} C$$

$$K_\phi = \frac{3\rho V^2 I_0}{z_0}, \quad C = \rho V I_0, \quad C'_\phi = 2 \frac{\zeta_0}{\omega_0} K_\phi, \quad (2)$$

$$m'_\phi = \frac{\zeta_0}{\omega_0} C$$

In the above notified equations, V is the shear wave velocity for the sway and torsional motions and the dilatational wave velocity for the rocking motions. ρ is the specific mass of the soil and z_0 is a parameter that depends on the soil's property (Wolf 1994). A_0 is the area, I_0 is the area moment of inertia, ζ_0 is the damping ratio and ω_0 is the fundamental frequency of the soil-structure system. In the SSI model, three soil types are used such as hard clay (shear wave velocity, $V_s=1000$ m/s), stiff clay (shear wave velocity, $V_s=600$ m/s) and soft clay (shear wave velocity, $V_s=300$ m/s), which contemplates the real site conditions of the OWT jacket support structure. The specific mass (1900 kg/m^3), damping ratio (0.05), Poisson's ratio (0.47) have been considered same for all clay soil profiles.

2.4 Incident angle of earthquake

By taking into consideration the general two components earthquake excitation, prescribed by the traditionally recorded accelerations $\ddot{u}_x(t)$ and $\ddot{u}_y(t)$ along the reference axes x and y successively. For the multi

degree of freedom system, the equation of motion of the linear time history analysis can be shown by Eq. (3)

$$\mathbf{M}\ddot{\mathbf{u}}(t) + \mathbf{C}\dot{\mathbf{u}}(t) + \mathbf{K}\mathbf{u}(t) = -\mathbf{P}_{eff}(t) \quad (3)$$

where \mathbf{M} , \mathbf{C} and \mathbf{K} are the mass, damping and stiffness matrices of the structure, distinctively, $\mathbf{P}_{eff}(t)$ represents the earthquake effective force vector and \mathbf{u} , $\dot{\mathbf{u}}$, $\ddot{\mathbf{u}}$ are the displacement, velocity and acceleration vectors respectively of the structural response. $\mathbf{P}_{eff}(t)$ can be expressed by Eq. (4)

$$\mathbf{P}_{eff}(t) = -\mathbf{M}[\mathbf{I}_{EW}\ddot{u}_{EW}(t) + \mathbf{I}_{NS}\ddot{u}_{NS}(t)] \quad (4)$$

whereas $\ddot{u}_{EW}(t)$ and $\ddot{u}_{NS}(t)$ are the two rotationally transformed horizontal components (Boor *et al.* 2006, Boor 2010) of $\ddot{u}_x(t)$ and $\ddot{u}_y(t)$ along the reference axes east-west (EW) and north-south (NS) directions successively. Moreover, \mathbf{I}_{EW} and \mathbf{I}_{NS} are the influence vectors joining to the degrees of freedom of the structure to the ground motion components $\ddot{u}_{EW}(t)$ and $\ddot{u}_{NS}(t)$. In Fig. 4, R_x is the scalar vector of $\ddot{u}_x(t)$ and R_y is the scalar vector of $\ddot{u}_y(t)$, whereas actual ground motion components are in the bi-directional excitation (Fujita and Takewaki 2010). Therefore, R_0 is the resultant vector of R_x and R_y with respect to the reference axes (x , y). These components satisfy the following Eqs. (5)-(6)

$$R_0(t) = R_x(t) \cos \alpha(t) + R_y(t) \sin \alpha(t) \quad (5)$$

$$\alpha(t) = \tan^{-1} \left(\frac{R_y(t)}{R_x(t)} \right) \quad (6)$$

Here, $\alpha(t)$ is the angle between the vectors R_0 and R_x , which is expressed as the time dependent variable. In Eqs. (7)-(8), $R_{EW}(\theta, t)$ is the scalar vector of $\ddot{u}_{EW}(t)$ and $R_{NS}(\theta, t)$ is the scalar vector of $\ddot{u}_{NS}(t)$. They are the rotated components of the original recorded horizontal components

$$R_{EW}(\theta, t) = R_0(t) \cdot \cos[\alpha(t) - \theta] \quad (7)$$

$$R_{NS}(\theta, t) = R_0(t) \cdot \sin[\alpha(t) - \theta] \quad (8)$$

Fig. 4(b) shows the plan view of the OWT, where C_M is the center mass of the structure. The acceleration time history 2674 load steps of bi-directional El Centro earthquake with an equal spacing and maximum PGA 0.34 g has been simulated between 0° and 165° considering 15° incremental interval since the remaining orientations from 180° to 360° produced identical values due to symmetry. A total of 12 pair sets time history accelerations have been

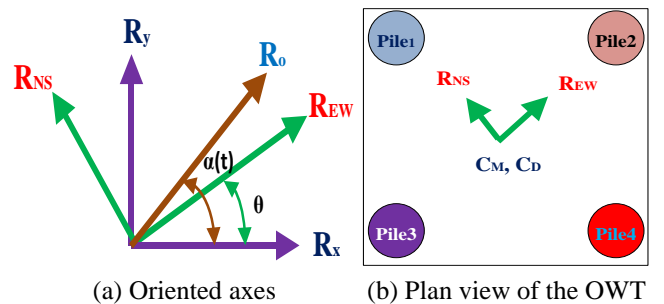
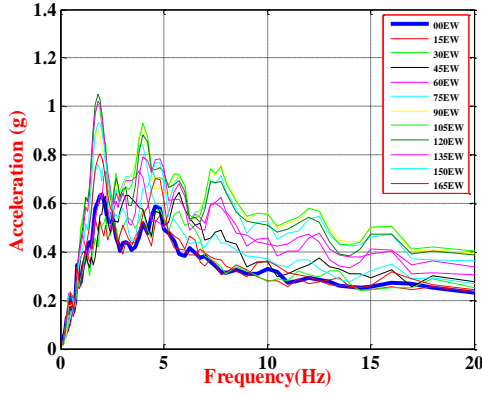
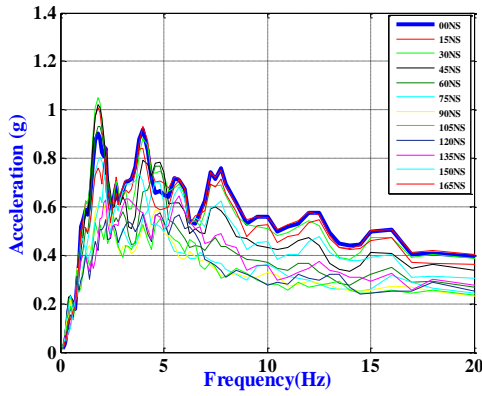


Fig. 4 Determination of incident angle



(a) EW direction



(b) NS direction

Fig. 5 Transformed acceleration response spectra at 5% damping

applied and the comparison of response spectrums of the input excitations is shown in Fig. 5.

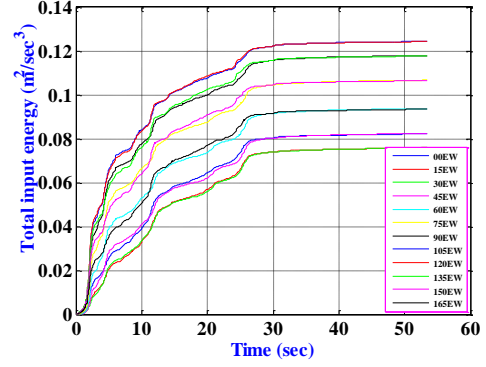
2.5 Wavelet analysis

The discrete wavelet transform has been used among two methods, such as the continuous wavelet transform and the discrete wavelet transform, which is more advantageous compare to the continuous wavelet transform and represents profound characteristics of a signal (Iyama and Kuwamura 1999).

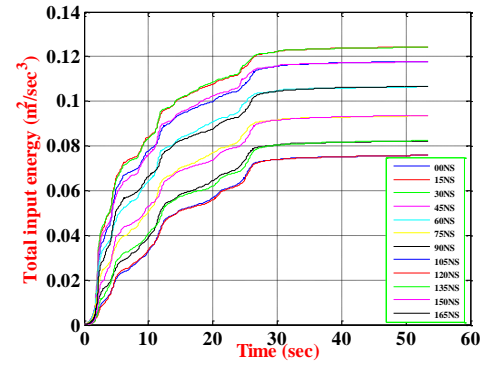
The total energy of a certain earthquake will remain same, but the energy of the dynamic response of the different structures will be different. In that case, the dynamic response of the OWT has been analyzed as a discrete signal through wavelet transform following this energy principle (Walker 1999), which is shown in Eq. (9)

$$E = \Delta t \sum_{t=0}^t A_0^2(t) = \Delta t \sum_{t=0}^t \left(\sum_{j=1}^n d_j(t) \right)^2 \quad (9)$$

Here, A_0 is the discrete signal of acceleration response of the structure due to the earthquake loads and $\Delta(t)$ is the time step of this signal. The acceleration response signal has been transformed into the discrete signal by the wavelet decomposition process. The process first splits the original



(a) EW direction



(b) NS Direction

Fig. 6 Time history of total energy of the input excitations

acceleration signal into two parts by passing through the two complimentary filters, such as the approximation $\{a(t)\}$ and the detail $\{d(t)\}$, where both depend on particular number of level (j) representing the particular range of frequency of the signal. The total number of decomposition is denoted by n in Eq. (9). The decomposition process is expressed as Eq. (10)

$$A_j(t) = a_{j+1}(t) + d_{j+1}(t) \quad (10)$$

In this study, 10th order Daubechies mother wavelet (Daubechies 1992) has been used as a basis wavelet function. The details components of the original signal based on linear combination of the wavelet basis functions can be presented by Eq. (11)

$$d_j(t) = \sum_{k=-\infty}^{\infty} c_{j,k} \psi_{j,k} = \sum_{k=-\infty}^{\infty} c_{j,k} \left\{ 2^{\frac{j}{k}} \psi(2^j t - k) \right\} \quad (11)$$

where $\psi_{j,k}$ and $c_{j,k}$ are the basis wavelet function and corresponding wavelet co-efficient respectively and k is the time scale index.

Consequently, as a time domain signal, an earthquake acceleration itself can represent the total input energy of the earthquake excitations. Fig. 6, illustrates the time history of the total energy response of different input earthquake excitations.

2.6 Fragility analysis

Fragility curves are most commonly used in the seismic analysis as they establish an influential means of the physical relation between the seismic hazard intensity and the probability of exceeding predefined limit state. For fragility curve analysis, this study has conducted multiple stripe analysis (MSA) and there is no need to persuade the analysis up to specific intensity measure amplitude. Wherein, all ground motion, causing collapse, are shortly succinct. For each fragility curve the parameters have been independently calculated by means of the maximum likelihood function, which can be depicted by Eq. (12) (Baker 2014)

$$\{\hat{\theta}, \hat{\beta}\} = \arg \max_{\theta, \beta} \sum_{j=1}^m \left\{ \ln \binom{n_j}{z_j} + z_j \ln P(a_i) + (n_j - z_j) \ln(1 - P(a_i)) \right\} \quad (12)$$

where P presents the fragility curve for specific state of the damage at PGA (which is a_i) will cause the structure to collapse. $\hat{\theta}$ and $\hat{\beta}$ denote the median and the lognormal standard deviation respectively for calibration of Eq. (13). After getting the analysis data, the fragility curve has been constructed by using Eq. (12), where $\hat{\theta}$ and $\hat{\beta}$ denote the fragility functions. In this procedure, the initial choices should not be revision but they could be altered if needed. So, the initially assumed values of $\hat{\theta}$ and $\hat{\beta}$ are 0.8 and 0.4, that means, here, beta value has been taken as 40%. Under current lognormal cumulative distribution function $P(a)$ takes the following analytical form

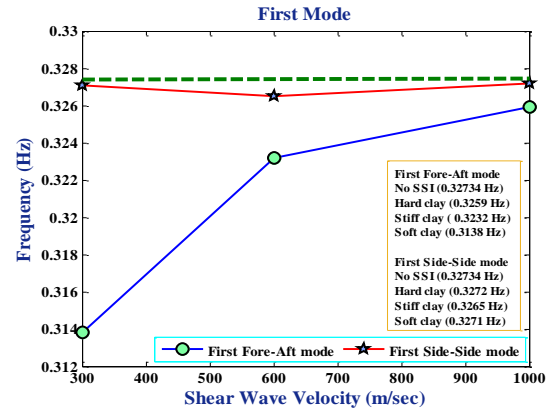
$$P(a) = \Phi \left(\frac{\ln(a/\theta)}{\beta} \right) \quad (13)$$

Here $\Phi(\)$ is the standardized cumulative normal distribution function (CDF), θ (theta) is the median of the fragility function and β (beta) is the log standard deviation of the fragility curves for the damage state. Moreover, a represents the PGA (0.1 g, 0.2 g ...) which has been distributed log normally and at each intensity level PGA is a_i , the structural analysis has generated some number of collapses out of a total number of ground motions. Here, i has been increased from 0 to 1 at incremental interval 0.1 PGA. Therefore, the number of collapses has been counted owing to the selected earthquakes at each PGA levels. After that, this collapses number has been divided by their corresponding number of earthquakes, which can be prescribed as observed fraction of collapses. The appropriate fitting technique for the observed fraction of collapses uses the maximum likelihood method (Shinozuka *et al.* 2000, Baker and Cornell 2005, Straub and Der Kiureghian 2008).

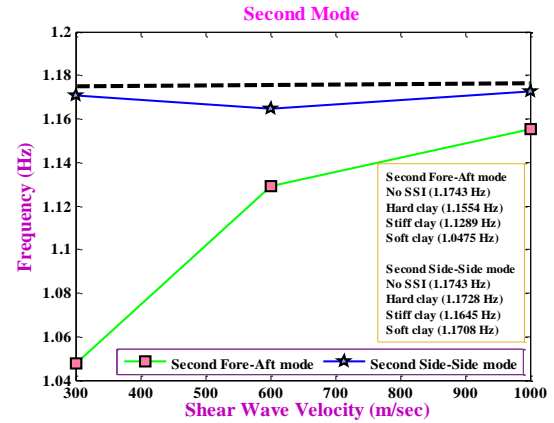
3. Numerical analysis

3.1 Natural frequencies

Modal analysis has been transacted to evaluate the effects of the SSI on the fundamental period of the OWT



(a) First mode of structural models



(b) Second mode of structural models

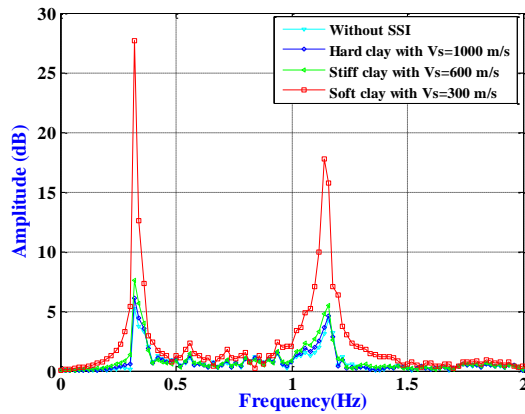
Fig. 7 Natural frequency of OWT with SSI

resting on the three different clay sites and the fixed base OWT. Fig. 7 illustrates the variation of the fundamental frequencies of the structure by considering the SSI effects. Certain results delineate that the first mode natural frequency (0.3138 Hz) of the structure with the soft clay flexible base is 4.12 % smaller than the frequency (0.3273 Hz) of the structure without the SSI. In the case of other two models, the reduction of natural frequencies is less than 1%. Besides, the frequencies in the second mode have decreased by 1.89%, 4% and 10.47% for three site conditions hard clay, stiff clay and soft clay successively. Although the changes of natural frequencies are not so significant for the effects of SSI, further analysis results of this paper give a profound demonstration of the SSI effects.

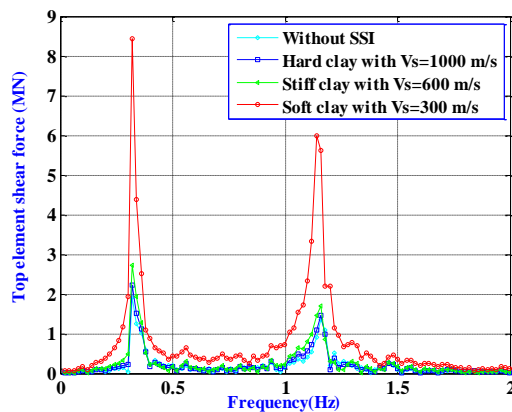
As it is within expectation that the smallest natural frequency can be found for 300 m/s soil type for the first mode and second mode. However, only the difference of natural frequency cannot characterize the effects of SSI on the OWT, comparisons of other results such as shear forces and moment responses, frequency response curves and energy responses can also implicitly demonstrate the effects of SSI. Further discussion will be carried out with respect to these analysis results.

3.2 Validation of earthquake analysis

As it has been mentioned before, static wind and wave



(a) FFT at tower top node

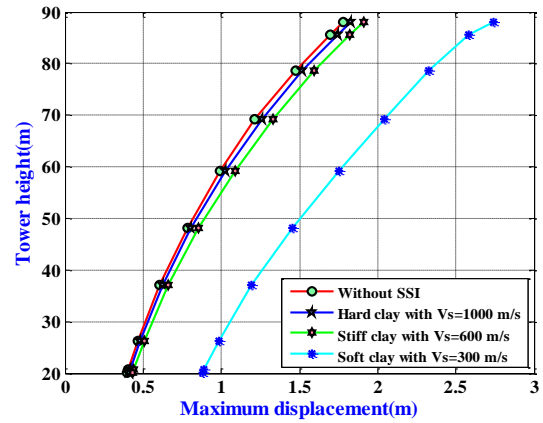


(b) FFT at tower top element

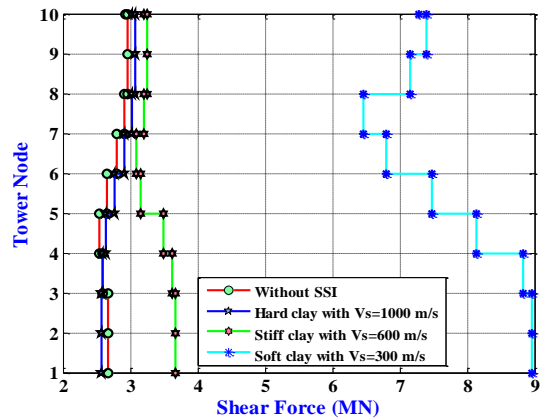
Fig. 8 Earthquake response validation

loads have been applied at the tower nodes and the jacket nodes of the structure successively, a static analysis has been performed considering these loads. The four structural models have been subjected to the linear transient analysis, which has been initiated from the previous static analysis case. To conduct the numerical time history analysis, Newmark- β method has been applied with the 5% structural damping ratio by using Rayleigh proportional damping. For the validation purpose of the seismic responses of several models with the SSI, the El Centro earthquake (1940) has been used in this investigation, fast Fourier transform (FFT) curves for the acceleration response Fig. 8(a) and for the shear force response Fig. 8(b) at the tower top node and element have been plotted respectively.

Results for the plausibility check are presented in Figs. 8(a)-(b), which shows reasonable maximum amplitude at the frequencies of two fundamental modes (first and second) of the four distinctive structural models. In the case of acceleration response, amplitudes increase further by 1.25 times, 2 times and 7 times of no SSI along with the decreasing shear wave velocities, 1000 m/s, 600 m/s and 300 m/s distinctively with reference to the fixed base. Besides, concerning the FFT for the shear force response, Fig. 8(b) shows the similar behavior. In both cases, the results for the hard clay condition are expected to close to the fixed base condition.



(a) Maximum lateral displacement

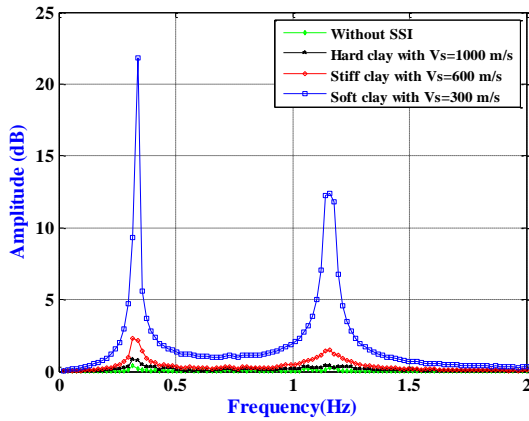


(b) Maximum shear force

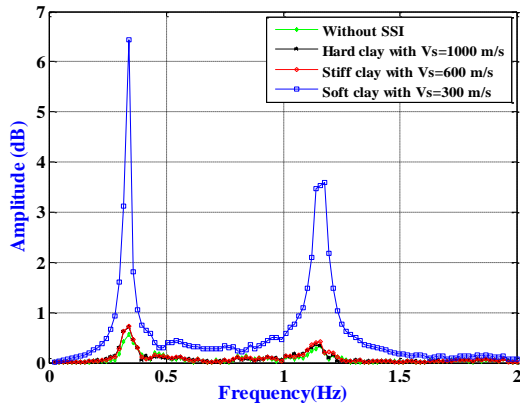
Fig. 9 Maximum lateral displacement and shear force response of the OWT under El Centro earthquake

Fig. 9 exhibits the lateral displacements and the shear forces for the El Centro earthquake at different tower height to demonstrate the comparison of the SSI effects. In the Fig. 9(b), the tower nodes from bottom to the top of the tower have been defined by gradual numbering from 1 to 10. Since, the uncertainty of the SSI is clearly designated for the model with soft clay (V_s 300 m/s) in the FFT curve, regarding the case of the lateral displacements and the shear forces, the same model also displays the significant influence of SSI rather than the other two models. The variation of lateral displacements of the top node illustrated in Fig. 9(a) increase further by 6.70%, 20% and 99.29 % for hard, stiff and soft clay respectively compare to the fixed base OWT. Similarly, in the case of shear forces, tower top shear forces increase by 7%, 14% and more than 100% along with the decreasing value of shear wave velocity of the soil model with respect to the fixed base OWT. In addition, the bottom of the tower shows the effective amount of changes in the lateral displacements and the shear forces due to the SSI effects comprehensively.

Before the study has verified the earthquake responses of the structure, when SSI has been considered. Still, it is required to prove the substantiation of the earthquake responses taking into account earthquake incidence. Therefore, FFT for earthquake acceleration responses of the OWT due to oriented input seismic excitations has been



(a) FFT at EW Direction



(b) FFT at NS direction

Fig. 10 Earthquake response validation considering earthquake incidence

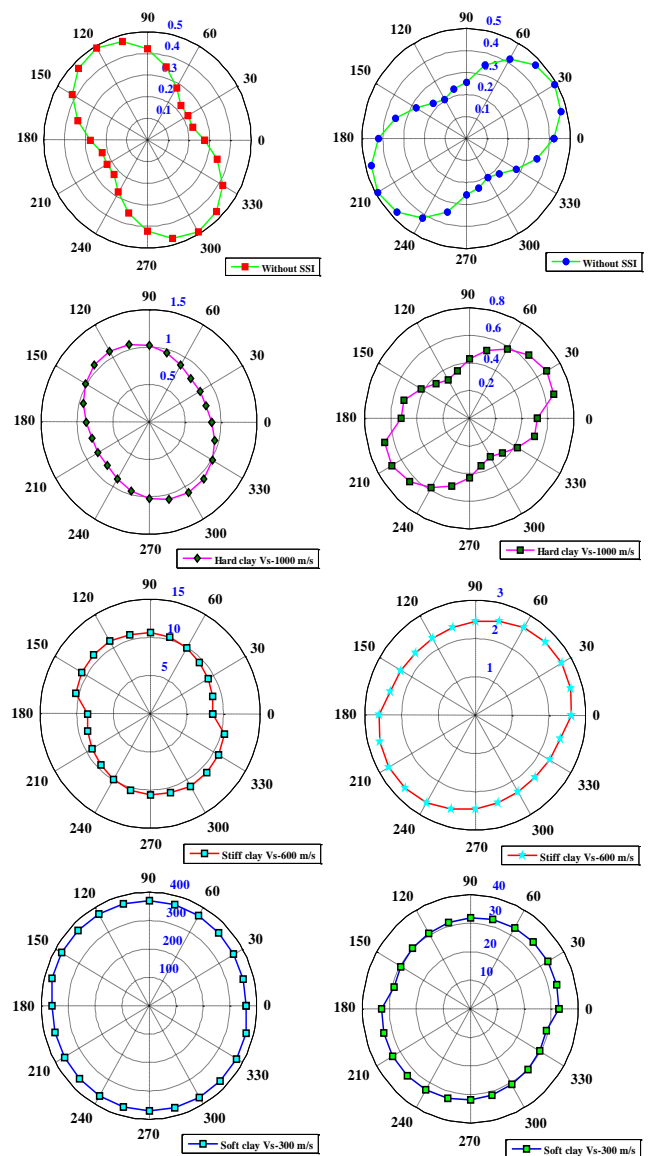
Table 4 EW directional total maximum energy

Degree	No SSI (m ² /sec ³)	Hard clay (m ² /sec ³)	Stiff clay (m ² /sec ³)	Soft clay (m ² /sec ³)
0°	0.28	0.88	8.51	359.33
15°	0.22	0.82	8.79	360.84
30°	0.23	0.83	9.14	362.85
45°	0.23	0.83	9.54	365.15
60°	0.28	0.88	9.95	367.47
75°	0.35	0.95	10.34	369.66
90°	0.42	1.02	10.66	371.52
105°	0.47	1.07	10.74	372.92
120°	0.49	1.09	10.96	373.76
135°	0.47	1.07	10.91	374.02
150°	0.42	1.02	10.73	373.73
165°	0.35	0.95	10.44	372.93

plotted (Fig. 10). In that case only one arbitrary angle 45° has been chosen for the validation purpose that represents all other angles. Recorded El Centro ground motion has been oriented by 45° angle according to section 2.4. Herein, FFTs at both directions (EW and NS) are governed by the fundamental natural frequencies, which adequately proves the verification of the seismic responses of the structure with the consideration of earthquake incidence.

Table 5 NS directional total maximum energy

Degree	No SSI (m ² /sec ³)	Hard clay (m ² /sec ³)	Stiff clay (m ² /sec ³)	Soft clay (m ² /sec ³)
0°	0.42	0.52	2.61	32.88
15°	0.47	0.67	2.69	33.16
30°	0.49	0.68	2.72	33.26
45°	0.47	0.65	2.70	33.16
60°	0.42	0.58	2.64	32.88
75°	0.35	0.51	2.55	32.44
90°	0.26	0.43	2.45	31.89
105°	0.23	0.36	2.37	31.28
120°	0.21	0.32	2.32	30.68
135°	0.23	0.36	2.31	30.12
150°	0.28	0.43	2.33	29.67
165°	0.35	0.52	2.38	29.32



(a) EW direction

(b) NS direction

Fig. 11 Total maximum energy (m²/sec³) of acceleration response

3.3 Influence of earthquake incidence

A total of 12 cases has been analyzed for particular group of earthquake motions with two horizontal acceleration components when the incidence, θ has been increased by 15° interval from 0° to 165° . Corresponding to the section (2.6), the wavelet transformation has been performed to calculate the total energy of the structure for each oriented input acceleration. The calculation results are listed in Tables 4-5 and also graphically shown in Fig. 11. The acquired results profoundly depict that, the total energy of the structure increases, while shear wave velocity reduces. As a consequence, the most destructive behavior of the model incorporated with soft clay with respect to other three models, which is quite reasonable because of the lower natural frequency of the structural model. On the other side, the fixed base structure is significantly influenced by the incidence of earthquake by showing an indicatory variation of the total output energy at different incident angles. According to the analysis, the total energy is minimum for 0° to 60° incident angle and maximum for 90° to 150° at EW direction. In the case of NS direction, the model behaves exactly the opposite.

3.4 Risk assessment by fragility analysis

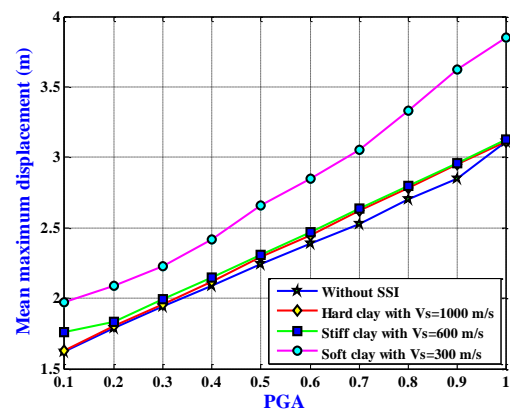
The present approach has been used four structural models; i.e., (with the SSI and without the SSI). In the SSI model, three different soil types have been used to take into consideration the SSI effects on the seismic responses of the OWT for different soil properties i.e., hard clay ($V_s = 1000$ m/s), stiff clay ($V_s = 600$ m/s) and soft clay ($V_s = 300$ m/s). Furthermore, multiple time history analysis has been conducted for the evaluation of uni-directional and bi-directional seismic responses of the OWT structure associated with the SSI at multiple intensity levels of each ground motion separately. 12 sets of input earthquake accelerations considering different incident angle have been used. Every distinctive pair of the input ground motion at each incident angle (from 0° to 165°) has been normalized and scaled from the 0.1g to 1.0g at a progressive interval of 0.1 g. This investigation has endeavored to present the SSI

Table 6 Mean displacements of structural models subjected to uni-direction excitation

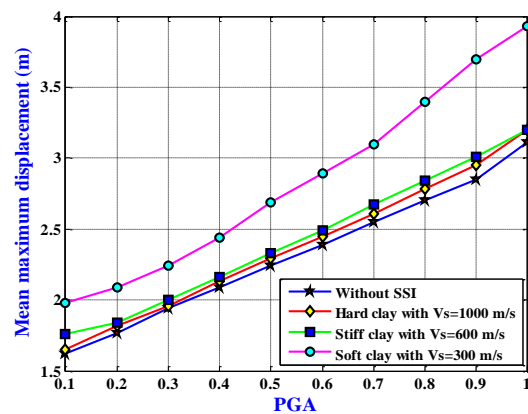
PGA	No SSI (m)	Hard clay (m)	Stiff clay (m)	Soft clay (m)
0.10	1.62	1.63	1.76	1.97
0.20	1.79	1.80	1.83	2.09
0.30	1.94	1.96	1.99	2.23
0.40	2.09	2.12	2.15	2.42
0.50	2.24	2.29	2.31	2.66
0.60	2.39	2.45	2.47	2.85
0.70	2.53	2.62	2.64	3.05
0.80	2.70	2.78	2.80	3.33
0.90	2.85	2.95	2.96	3.62
1.00	3.11	3.11	3.13	3.85

Table 7 Mean displacements of structural models subjected to bi-direction excitation

PGA	No SSI (m)	Hard clay (m)	Stiff clay (m)	Soft clay (m)
0.10	1.62	1.65	1.76	1.98
0.20	1.77	1.82	1.84	2.09
0.30	1.94	1.96	2.00	2.24
0.40	2.09	2.13	2.16	2.39
0.50	2.24	2.29	2.33	2.44
0.60	2.39	2.45	2.49	2.69
0.70	2.55	2.61	2.67	3.10
0.80	2.70	2.78	2.84	3.40
0.90	2.85	2.95	3.01	3.70
1.00	3.11	3.20	3.20	3.93



(a) Uni- direction



(b) Bi- direction

Fig. 12 Mean maximum displacement demands

effects with different soil profiles on the lateral displacements of the structure to single and bi-directional seismic excitations distinctively.

Tables 6-7 schematically illustrate the mean of maximum lateral displacements recorded at the tower top node of the structure associated with fixed and flexible boundary conditions subjected to uni-directional and bi-directional excitations separately. In the same manner Fig. 12 gives a graphical representation of the variation of mean maximum displacements with the incremental PGA.

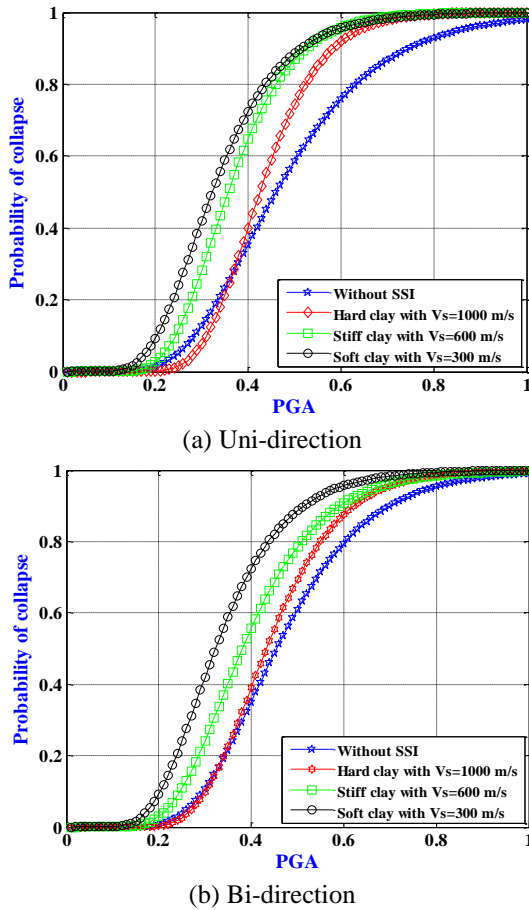


Fig. 13 Fragility curves

Table 8 Fragility functions of different cases

Structural model	Single excitation		Double excitation	
	$\hat{\theta}$	$\hat{\beta}$	$\hat{\theta}$	$\hat{\beta}$
No SSI	0.4610	0.3769	0.4553	0.3350
Hard Clay	0.4255	0.2455	0.4328	0.2830
Stiff Clay	0.3571	0.3007	0.3812	0.3416
Soft Clay	0.3228	0.3618	0.3228	0.3618

The SSI effects are found to be higher on the structure for the soft clay type, which makes around 15% (single excitation) and 24% (double excitation) differences in soft clay type and no SSI at high intensity level (1.0 PGA). Moreover, the structure brings incremental changes in the mean displacements while the intensity level of ground motion increases for all soil type conditions.

For the fragility analysis, the target displacement has been estimated by executing pushover analysis of the OWT structure, which is the key factor to estimate the collapses of the structure under the selected ground motions at different intensity level. Two cases have been considered with different soil profiles, where 2.113 m taken as displacement limit state. Figs. 12(a)-(b) represent the fragility curves of the structure for all boundary conditions (no SSI, hard clay, stiff clay and soft clay). In each graph, the probability of exceeding denotes by the y-axis, while the x-axis presents the PGA.

From the attained graphs (Fig. 13) it can be described that in both cases, the structure associated with soft clay SSI model shows the highest probability of limit state exceedance, which is about 33% higher than the fixed base boundary condition. The reason of the higher failure probability of the model for soil type with respect to other models is because of the maximum lateral displacement of the model for same soil condition. Besides, it can be compared the level of collapse between single and double excitation, the structures (with hard clay and soft clay) show moderate incremental probability failure in case of single excitation in comparison to the second case. Table 8 lists the parameters ($\hat{\theta}$ and $\hat{\beta}$) that define the fragility functions for the seismic assessment of the OWT structure.

4. Conclusions

This research has investigated the influence of SSI on the OWT subjected to earthquake incidence. Two different perspectives have been considered, (a) the output structural energy response and (b) probability of collapse. To accomplish the modeling of the SSI, the Voigt viscoelastic cone model has been selected. The earthquake incidence has been determined through the numerical mathematical model. In order to estimate the total energy of input earthquake excitations and the energy of the structural dynamic responses under the ground motion, the wavelet transformation has been used. To establish the analytical fragility curves corresponding to incremental PGA of each selected ground motions for the four established structural models, a parametric execution of the time history analysis has been performed. This research also shows comparisons of the probability of exceedance of the structure without SSI and the structure with different clay site conditions under uni-directional and bi-directional excitations. Based on the obtained results the major conclusions are:

1. The SSI effects show significant influence on the OWT seismic responses. The indicative impact of the SSI can be noticed, especially in the performance of the model with soft clay SSI corresponding to analysis results of the maximum lateral displacements and the shear forces.
2. The numerical analysis results delimitate that the model with soft clay SSI shows larger values in the case of total output energy rather than other three models under input earthquake excitations. However, the variation of the total output energy for the earthquake incidence is prominently visible for the fixed base structure.
3. The observation demonstrates that the soil profile tends to deduct the efficiency of the OWT system and increases the probability of collapse, especially for the soft clay. The certain research suggests that the SSI should also be considered because the probability of collapse of key components of the OWT system under seismic incidence may be significantly underestimated if the SSI effects are not considered.

Further research is required with the consideration of dynamic wind and wave loads interaction instead of static

loads. As the irregular structures show the desperate behavior rather than regular structures while the structures subjected to earthquake incidence, it is necessary to understand the influence of SSI on irregular OWT structures induced by earthquake incidence.

Acknowledgements

The Authors gratefully acknowledge the financial support of the Korea Institute of Energy Technology Evaluation and Planning (KETEP) and the Ministry of Trade, Industry & Energy (MOTIE) of the Republic of Korea (No. 20153030023760).

References

- Abhinav, K.A. and Saha, N. (2015), "Coupled hydrodynamic and geotechnical analysis of jacket offshore wind turbine", *Soil Dyn. Earthq. Eng.*, **73**, 66-79.
- Adhikari, S. and Bhattacharya, S. (2011), "Vibration of wind turbines considering soil-structure interaction", *Wind Struct.*, **14**(2), 85-112.
- Bhattacharya, S., Cox, J.A., Lombardi, D. and Wood, D.M. (2013), "Dynamics of offshore wind turbines supported on two foundations", *Proc. Inst. Civ. Engineers*, **166**(2), 159-169.
- Bradley, B.A. (2010), "A generalized conditional intensity measure approach and holistic ground-motion selection", *Earthq. Eng. Struct. D.*, **39**(12), 1321-1342.
- Baker, J.W. and Cornell, C.A. (2005), "A vector-valued ground motion intensity measure consisting of spectral acceleration and epsilon", *Earthq. Eng. Struct. D.*, **34**(10), 1193-1217.
- Baker, J.W. (2014), "Efficient analytical fragility function fitting using dynamic structural analysis", *Earthq. Spectra*, **31**(1), 579-599.
- Boor, D.M., Lamprey, J.W. and Abrahamson, N.A. (2006), "Orientation-independent measures of ground motion", *Bull. Seismol. Soc. Am.*, **96**(4A), 1502-1511.
- Boor, D.M. (2010), "Orientation-independent, nongeometric-mean measures of seismic intensity from two horizontal components of motion", *Bull. Seismol. Soc. Am.*, **100**(4), 1830-1835.
- Cai, Y.X., Gould, P.L. and Desai, C.S. (1999), "Nonlinear analysis of 3D seismic interaction of soil-pile-structure systems and application", *Eng. Struct.*, **22**(2), 191-199.
- Chatterjee, P. and Basu, B. (2004), "Wavelet-based non-stationary seismic rocking response of flexibility supported tanks", *Earthq. Eng. Struct. D.*, **33**(2), 157-181.
- Daubechies, I. (1992), *Ten lectures on wavelets*, Society for Industrial and Applied Mathematics, Philadelphia, PA, USA.
- Fukumoto, Y. and Takewaki, I. (2015), "Critical earthquake input energy to connected building structures using impulse input", *Earthq. Struct.*, **9**(6), 1133-1152.
- Fujita, K. and Takewaki, I. (2010), "Critical correlation of bi-directional horizontal ground motions", *Eng. Struct.*, **32**(1), 261-272.
- Ghaffar-Zade, M. and Cahpel, F. (1983), "Frequency-independent impedance of soil-structure system in horizontal and rocking modes," *Earthq. Eng. Struct. D.*, **11**(4), 523-540.
- Hajizadeh, A.R., Salajegheh, J. and Salajegheh, E. (2016), "Performance evaluation of wavelet and curve let transforms based-damage detection of defect types in plate structures", *Struct. Eng. Mech.*, **60**(4), 667-691.
- He, W.Y. and Zhu, S. (2015), "Adaptive-scale damage detection strategy for plate structures based on wavelet finite element model", *Struct. Eng. Mech.*, **54**(2), 239-256.
- Hussan, M., Sharmin, F. and Kim, D. (2017), "Multiple tuned mass damper based vibration mitigation of offshore wind turbine considering soil-structure interaction", *China Ocean Eng.*, **31**(5), 1-11.
- Iyama, J. and Kuwamura, H. (1999), "Application of wavelets to analysis and simulation of earthquake motions", *Earthq. Eng. Struct. D.*, **28**(3), 255-272.
- Iervolino, I., Giorgio, M., Galasso, C. and Manfredi, G. (2010), "Conditional hazard maps for secondary intensity measures", *Bull. Seismol. Soc. Am.*, **100**(6), 3312-3319.
- IEC 61400-1:2005+AMD1:2010 CSV consolidated version, *Wind Turbine Design Requirements*, part-1.
- IEC 61400-3:2009, *Design Requirements for Offshore Wind Turbine*, part-3.
- Jayalekshmi, B.R., Thomas, A. and Shivashankar, R. (2014), "Dynamic soil-structure interaction studies on 275 m tall industrial chimney with openings", *Earthq. Struct.*, **6**(6), 233-250.
- Jonkman, J., Butterfield, S., Musial, W. and Scott, G. (2009), "Definition of a 5-MW reference wind turbine for offshore system development", Technical Report NREL/TP-500-38060, National Renewable Energy Laboratory (NREL), USA.
- Karantoni, F., Tsionis, G., Lyrantzaki, F. and Fardis, M.N. (2014), "Seismic fragility of regular masonry buildings for in-plane and out-of-plane failure", *Earthq. Struct.*, **6**(6), 689-713.
- Kuo, Y., Achmus, M. and Rahman, A.K. (2012), "Minimum embedded length of cyclic horizontally loaded monopiles", *J. Geotech. Geo-environ. Eng.*, **138**(3), 357-363.
- Kim, D.H., Lee, S.G. and Lee, I.K. (2015), "Dynamic reliability analysis of offshore wind turbine support structure under earthquake", *Wind Struct.*, **21**(6), 609-623.
- Kuwamura, H., Kirino, Y. and Akiyama, H. (1994), "Prediction of earthquake energy input from smoothed Fourier amplitude spectrum", *Earthq. Eng. Struct. D.*, **23**(10), 1125-1137.
- Kim, D.H., Lee, S.G. and Lee, I.K. (2014), "Seismic fragility analysis of 5 MW offshore wind turbine", *Renewable Energy*, **65**, 250-256.
- Kojima, K. and Takewaki, I. (2015), "Critical earthquake response of elastic-plastic structures under near-fault ground motions (Part 1: Flung-step input)", *Front. Built Environ. (Specialty Section: Earthquake Engineering)*, **1**, 12.
- Kojima, K. and Takewaki, I. (2016), "Closed-form critical earthquake response of elastic-plastic structures on compliant ground under near-fault ground motions", *Front. Built Environ. (Specialty Section: Earthquake Engineering)*, **2**, 1.
- Li, H.N., He, X.Y. and Yi, T.H. (2009), "Multi-component seismic response analysis of offshore platform by wavelet energy principle", *Coast. Eng.*, **56**(8), 810-830.
- Li, H.N. and Sun, H.M. (2003), "Application of wavelet analytical method to civil engineering", *World Earthq. Eng.*, **19**(2), 16-22.
- Menuin, C. and Kiureghian, A.D. (1998), "A replacement for the 30%, 40% and SRSS rules for multicomponent seismic analysis", *Earthq. Spectra*, **14**(1), 153-163.
- Melhem, H. and Kim, H. (2003), "Damage detection in concrete by Fourier and wavelet analysis", *J. Eng. Mech.*, ASCE, **129**(5), 571-577.
- Mohammad, A.A., William, S. and Jeffery, V. (2016), "Fragility analysis of a 5-MW NREL wind turbine considering aero-elastic and seismic interaction using finite element method", *Finite Elem. Anal. Des.*, **120**, 57-67.
- Meek, W. and Wolf, J.P. (1993a), "Cone models for nearly incompressible soil", *Earthq. Eng. Struct. D.*, **22**(8), 649-663.
- Meek, W. and Wolf, J.P. (1993b), "Why cone model represents the elastic half space", *Earthq. Eng. Struct. D.*, **22**(9), 759-771.
- Nuta, E. (2010), "Seismic analysis of steel wind turbine towers in the Canadian environment", Master's Dissertation, University

- of Toronto, Canada.
- Nguyen, V.T. and Kim, D. (2013), "Influence of incident angles of earthquakes on inelastic responses of asymmetric-plan structures", *Struct. Eng. Mech.*, **45**(3), 373-389.
- Prowell, I., Elgamal, A. and Jonkman, J. (2009), "FAST simulation of wind turbine seismic response", *Presented at the 2009 Asian-Pacific Network of Centers for Earthquake Engineering Research (ANCER) Workshop Urbana-Champaign, Illinois*, 13-14.
- Smeby, W. and Kiureghian, A.D. (1985), "Modal combinations rules for multi-component earthquake excitation", *Earthq. Eng. Struct. D.*, **13**(1), 1-12.
- Shinozuka, M., Feng, M.Q., Lee, J. and Naganuma, T. (2000), "Statistical analysis of fragility curves", *J. Eng. Mech.*, **126**(12), 1224-1231.
- Straub, D. and Kiureghian, A.D. (2008), "Improved seismic fragility modeling from empirical data", *Struct. Safe.*, **30**(4), 320-336.
- Song, H., Damiani, R., Robertson, A. and Jonkman, J. (2013), "A new structural-dynamics module for offshore multimember substructures within the wind turbine computer-aided engineering tool FAST", *Presented at the 23rd International Ocean, Offshore and Polar Engineering Conference, International Society of Offshore and Polar Engineers, Anchorage, Alaska*.
- Uang, C.M. and Bertero, V.V. (1990), "Evaluation of seismic energy in structures", *Earthq. Eng. Struct. D.*, **9**(1), 77-90.
- Valamanesh, V. and Myers, A. (2014), "Aerodynamic damping and seismic response of horizontal axis wind turbine towers", *J. Struct. Eng.*, ASCE, **140**(11), 04014090.
- Vemula, N.K., DeVries, W., Fischer, T., Cordle, A. and Schmidt, B. (2010), *Design solution for the upwind reference offshore support structure*, Upwind deliverable D4.2.6 (WP4: offshore foundations and support structures), Ramboll Wind Energy.
- Wilson, E.L. and Butten, M. (1982), "Three-dimensional dynamic analysis for multi-component earthquake spectra", *Earthq. Eng. Struct. D.*, **10**(3), 471-476.
- Wolf, J.P. (1994), *Foundation vibration analysis using simple physical models*, Prentice-Hall, Englewood Cliffs, NJ.
- Walker, J.S. (1999), *A primer on wavelets and their scientific applications*, Chapman and Hall/CRC, New York.
- Zhu, D.S., Yu, L.S. and Liu, S.Z. (2000), "The study of earthquake input principal direction for irregular bridges", *J. Lanzhou Railway Univ.*, **19**, 631-636.